

# Topology optimization of multiphase elastic plates with Reissner-Mindlin plate theory

Thanh T. Banh<sup>1a</sup>, Dongkyu Lee<sup>\*1</sup>, Jaehong Lee<sup>1b</sup>, Joowon Kang<sup>2b</sup> and Soomi Shin<sup>3c</sup>

<sup>1</sup>Department of Architectural Engineering, Sejong University, Seoul 05006, Korea

<sup>2</sup>Department of Architecture, Yeungnam University, Gyeongsan 38541, Korea

<sup>3</sup>Research Institute of Industrial Technology, Pusan National University, Busan 46241, Korea

(Received December 20, 2017, Revised June 6, 2018, Accepted June 18, 2018)

**Abstract.** This study contributes to evaluate multiphase topology optimization design of plate-like elastic structures with constant thickness and Reissner-Mindlin plate theory. Stiffness and adjoint sensitivity formulations linked to Reissner-Mindlin plate potential energy of bending and shear are derived in terms of multiphase design variables. Multiphase optimization problem is solved through alternative active-phase algorithm with Gauss-Seidel version as an optimization model of optimality criteria. Numerical examples verify efficiency and diversity of the present topology optimization method of Reissner-Mindlin elastic plates depending on multiphase and Poisson's ratio.

**Keywords:** topology optimization; multiphase; Reissner-Mindlin plate; Q4 element approximation, adjoint sensitivity; Poisson's ratio

## 1. Introduction

In recent years, computer-aided topology optimization has been receiving increasing attention. Since the pioneering study (Bendsøe and Kikuchi 1988), topology optimization has made remarkable progress as an innovative numerical and design method, attracting an enormous amount of attention from the scientific community (Lee and Shin 2015a, b, Olyaie and Razfar 2013, Lee *et al.* 2016). It is a relatively new but rapidly expanding field of structural mechanics. It is used in an increasing rate in industrial applications and designing mechanical components such as manufacture field (Vatanabea *et al.* 2016, Liu and Ma 2016), laminated composite structures (Blasques and Stolpe 2012, Lund 2009), thermoelastic structures (Xia and Wang 2008), piezoelectric material (Noha and Yoon 2012), multi-functional designs (Chen *et al.* 2010, Chen *et al.* 2009) and other applications (Kutyłowski and Szwachlowski 2013, Goncalves *et al.* 2016). The reason of the feasibility is that it often achieves greater material savings and design improvements than shape optimization.

In actuality, thick plate bending model has a wider range of applicability than thin plate theory. Because thick plate theory, particularly using Reissner-Mindlin theory, is taken into account shear deformations through the thickness of a plate. Therefore, there are several works have studied

the optimization problem of topology optimization of thick plate. Indeed, Belblidia *et al.* (2001) presented a novel topology optimization algorithm for single- or three-layered artificial material model. Goo *et al.* (2016) studied optimal topologies for thin plate structures with bending stress constraints. Yan *et al.* (2016) studied optimal topology design of damped vibrating plate structures subjected to initial excitations. Nevertheless, adding hard materials to keep the same amount of total material may produce stiffer structures than single material (Tavakoli and Mohseni 2014, Zhou and Wang 2006).

In topology optimization fields, multi-material topology optimization is attractive part to finds optimal density distributions of different types of material in given conditions. Zhou and Wang (2007) introduced a phase field method for the multi-material structural topology optimization with a generalized Cahn-Hilliard model. Sigmund and Torquato (1997) introduced the design of materials with an extreme thermal expansion using three-phase topology optimization. Alonso *et al.* (2014) studied topology synthesis of multiple materials by using a multi Sequential Element Rejection and Admission (SERA) method. Yun and Youn (2017) investigated optimized topologies using multiple materials for viscoelastically damped structures under time-dependent loading. In this study, to discover multi-material density distributions, an alternating active phase algorithm of optimal criteria introduced by Tavakoli and Mohseni (2014) is considered. The multi-material-phase field approach is based on a Cahn-Hilliard equation, and a general method to solve multiphase structure topology optimization problems was presented by Zhou and Wang (2006, 2007). Therefore, this study focuses on the usage of multiple materials to topology optimization for approximation of plate structures using Reissner-Mindlin plate theory. In addition, adjoint

\*Corresponding author, Associate Professor  
E-mail: dongkyulee@sejong.ac.kr

<sup>a</sup> Ph.D. Student

<sup>b</sup> Professor

<sup>c</sup> Research Professor

sensitivity formulations of strain energy of Reissner-Mindlin plates are derived with respect to multi-material densities.

The obtained results are presented to demonstrate the success, performance, and effectiveness of the present method. This study contributes to engineers and designers the real-time design information for plate-like structures by using multi-material topology optimization.

The outlines of this study are as follows. This study begins in Section 2 with a brief of Reissner-Mindlin plate theory. The analysis models of multi-material topology problem including a stiffness formulation and sensitivity analysis of compliance for plates structures are formulated in Section 3. Section 4 presents a computation procedure of the present method. Numerical applications to verify the present method are discussed in Section 5. Finally, conclusions are shown in Section 6.

## 2. A brief of governing equations of Reissner-Mindlin plates

In this section, basic equations of Reissner-Mindlin plate theory are summarized. Let  $\Omega$  be the domain of a flat isotropic homogeneous thick plate,  $\Gamma$  is the boundary domain, and  $h$  is the thickness. The mid-plane of the plate is taken as the reference plane as shown in Fig. 1. The displacement field at any point of the plate is expressed as

$$\begin{aligned} u(x, y, z) &= -z\theta_x(x, y) \\ v(x, y, z) &= -z\theta_y(x, y) \\ w(x, y, z) &= w_0(x, y) \end{aligned} \quad (1)$$

where  $(u, v, w)$  are components of displacement at a general point in a domain.  $w_0$  is transverse deflection on a plate's middle surface, and  $(\theta_x, \theta_y)$  is rotations in  $x$  and  $y$  direction of a middle surface as shown in Fig. 2. Accordingly, bending and shear strain  $\kappa$  and  $\gamma$  are respectively written as follows

$$\kappa_{\alpha,\beta} = \frac{1}{2}(\theta_{\alpha,\beta} + \theta_{\beta,\alpha}), \quad \gamma_\beta = w_{,\beta} - \theta_\beta \quad (2)$$

where the subscripts  $\alpha$  and  $\beta$  range from  $x$  to  $y$ .

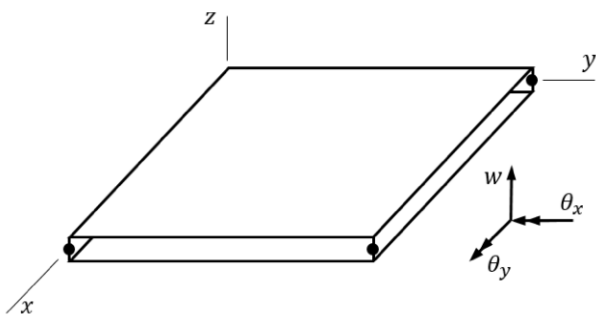


Fig. 1 A thick plate element with corner nodes showing typical nodal degree of freedom

The total energy  $\Pi$  of Reissner-Mindlin plate, based on potential energy for bending and shear, is stated as follows

$$\Pi = \frac{1}{2} \int_{\Omega} \kappa^T \mathbf{D}_b^T \kappa d\Omega + \frac{1}{2} \int_{\Omega} \gamma^T \mathbf{D}_s^T \gamma d\Omega + \Pi_{ext} \quad (3)$$

where  $\Pi_{ext}$  is the potential energy of applied loads. Material property tensors of bending and shear are respectively written as follows

$$\mathbf{D}_b = \frac{Et^3}{12(1-\nu^2)} \begin{bmatrix} 1 & \nu & 0 \\ \nu & 1 & 0 \\ 0 & 0 & (1-\nu)/2 \end{bmatrix}, \quad \mathbf{D}_s = tG\kappa \begin{bmatrix} 1 & 0 \\ 0 & 1 \end{bmatrix} \quad (4)$$

where shear modulus  $G = E/2(1+\nu)$ .  $E$  is Young's modulus and  $\nu$  is Poisson's ratio. Shear correction factor is chosen to be 5/6 for the purpose of removal of shear locking. In this study,  $t$  is constant to homogeneous thick plate.

The problem design domain  $\Omega$  is discretized into a finite number of quadrilateral isoparametric elements,  $\Omega = \sum_e \Omega_e$ . The sectional rotations and the transverse mid-surface displacements are bilinearly interpolated as

$$w = \sum_{j=1}^4 N_j w_j; \quad \theta_x = \sum_{j=1}^4 N_j \theta_{xj}; \quad \theta_y = \sum_{j=1}^4 N_j \theta_{yj} \quad (5)$$

where  $(w_j, \theta_{xj}, \theta_{yj})$  are nodal point values of variables  $(w, \theta_x, \theta_y)$  with  $j$ -th node. The curvature-displacement and shear strain-displacement relation are written as, respectively

$$\kappa = \mathbf{B}_b \mathbf{q}; \quad \gamma = \mathbf{B}_s \mathbf{q} \quad (6)$$

where  $\mathbf{q}_i = [w_i \ \theta_{xi} \ \theta_{yi}]^T$  and

$$\mathbf{B}_{bj} = \begin{bmatrix} 0 & N_{j,x} & 0 \\ 0 & 0 & N_{j,y} \\ 0 & N_{j,y} & N_{j,x} \end{bmatrix}; \quad \mathbf{B}_{sj} = \begin{bmatrix} N_{j,x} & N_j & 0 \\ N_{j,y} & 0 & N_j \end{bmatrix} \quad (7)$$

By using Eqs. (5)-(7), the stationary condition of variational expression Eq. (3) and the plate stiffness-displacement relationship are obtained as

$$(\mathbf{K}_b^e + \mathbf{K}_s^e) \mathbf{q} = \mathbf{F} \quad (8)$$

where  $\mathbf{F}$  is the global load vector.  $\mathbf{K}_b^e$  and  $\mathbf{K}_s^e$  are bending and shear stiffness matrix components, respectively, as follows

$$\mathbf{K}_b^e = \int \mathbf{B}_b^T \mathbf{D}_b \mathbf{B}_b d\Omega, \quad \mathbf{K}_s^e = \int \mathbf{B}_s^T \mathbf{D}_s \mathbf{B}_s d\Omega \quad (9)$$

### 3. Formulations of multi-material topology optimization of Reissner-Mindlin plates

#### 3.1 Multiphase topology optimization problem

We consider the minimum compliance based multi-material topology optimization problem within a design domain  $\Omega$  discretized by quadrilateral isoparametric finite element (Q4). Each subdomain  $\Omega_j$  ( $j = 1, 2, \dots, n$ ) can be materials or void as shown in a design domain schematic of multi-material topology optimization as described in Fig. 3.  $\Omega_s^m$  and  $\Omega_v^m$  are the solid domain of material and void domain in a multi-material problem, respectively.  $m$  denotes the number of multi-material. Relative densities of each element are design variables  $\alpha$  connected into a vector  $\alpha$ . Following Bendsøe and Sigmund (1999), void is considered as a separate material phase. In other words, multi-material topology optimization to find the optimal material distribution of  $n$  number of materials corresponding to find  $n+1$  material phases  $\alpha_i = \alpha_i(x)$  at each point  $x \in \Omega$ . In case of the minimum compliance multi-material topology optimization problem, the modified SIMP version of linear interpolation is used within the elasticity stiffness tensor for multi-material as follows

$$E(\alpha) = \sum_{i=1}^{n+1} \alpha_i^p E_i^0 \quad (10)$$

where  $p$  is penalization factor.  $E_i^0$  is elastic modulus corresponding to phase  $i$ -th.

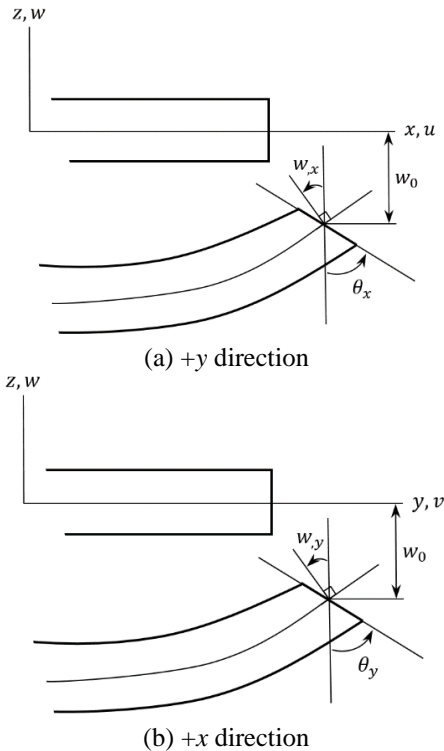


Fig. 2 Cross section view of deformed plate in two directions

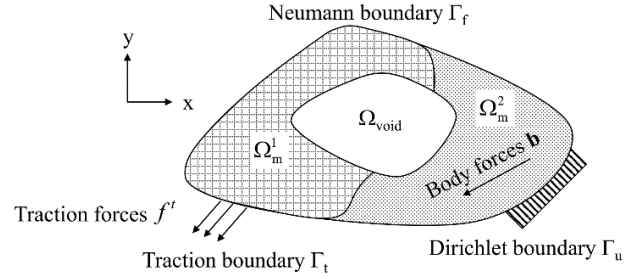


Fig. 3 A design domain schematic for multi-material topology optimization

According to alternating active phase algorithm, the multi-phase topology optimization problem is solved by converting multi-phase into  $p(p-1)/2$  binary phases sub-problem. Each binary sub-problem is a so-called active phase. This solver could be made by modification of the binary phase topology optimization algorithm. The modifications is carried out by replacing the binary phase material properties operator to a corresponding multiphase one and modifying structures of admissible design domain in the binary phase topology optimization algorithm. Two alternating active phase algorithm schemes are proposed by Tavakoli and Mohseni (2014). In this study, Gauss-Seidel version is considered due to preference of optimality criteria with single constraint. In this process of each sub-problem, only two phases denote as 'a' and 'b' are active at a time and the other phases are fixed. Overlaps are not allowed in a desired optimal design, thus summation of the densities at each point  $x \in \Omega$  should be equal to unity  $\sum_i \alpha_i = 1, i = 1, 2, \dots, p$ . The density summation of two active phases at each point  $x \in \Omega$  is then calculated as

$$\alpha_a(x) + \alpha_b(x) = 1 - \sum_{i=1, i \neq \{a,b\}}^{n+1} \alpha_i(x) \quad (11)$$

In each computational cell, the problem can be simplified in each binary phase topology optimization subproblem by taking the density of active phase 'a' as the only design variable. And then, the density of phase 'b' (or background phase) can be calculated by Eq. (11).

#### 3.2 Optimization model

The general mathematical formulation of structural multi-material topology optimization problem (Banh and Lee 2018) can be stated as follows

$$\begin{aligned} & \underset{\alpha}{\text{minimize}} : C(\alpha, \mathbf{U}) = \mathbf{U}^T \mathbf{K} \mathbf{U} \\ & \text{subject to} : \mathbf{K}(\alpha) \mathbf{U} = \mathbf{F} \\ & \int_{\Omega} \alpha_i dx \leq V_i \\ & 0 < \varepsilon_i \leq \alpha_i \leq 1 \end{aligned} \quad (12)$$

where  $C$  is structural compliance.  $\alpha_i$  is the density vector

for phase material  $i$ -th.  $V_i$  is the per-material volume fraction constraint with  $i=1:n+1$  such that the summation should be equal to unity  $\sum_i V_i = 1$ .  $\mathbf{K}$  is global stiffness matrix,  $\mathbf{F}$  is global load vector, and  $\mathbf{U}$  is global displacement vector. To avoid singularities in calculation processes of topology optimization, the problem is relaxed for densities between 0 and 1 by a very small lower bound non-zero value  $\varepsilon_i$ .

### 3.3 Stiffness and sensitivity formulation for Reissner-Mindlin plates

Substituting Eq. (10) into Eq. (9), the stiffness matrix is written as follows.

$$\mathbf{K}^e = \sum_{r=\{b,s\}} \mathbf{K}_r^e = \sum_{r=\{b,s\}} \int_{\Omega^e} \mathbf{B}_r^T \left( \sum_{k=1}^{n+1} \alpha_k^p \mathbf{D}_k^{r0} \right) \mathbf{B}_r d\Omega \quad (13)$$

where  $\mathbf{D}_k^{r0}$  with  $r=\{b,s\}$  are respectively the material property matrices of bending and shear corresponding to the  $k$ -th phase material, including Poisson's ratio  $\nu$ , constant thickness  $t$ , and nominal elastic modulus  $E_k^0$ ,

$$D_k^{0b} = \frac{E_k^0 t^3}{12(1-\nu^2)} \begin{bmatrix} 1 & \nu & 0 \\ \nu & 1 & 0 \\ 0 & 0 & (1-\nu)/2 \end{bmatrix} \quad (14)$$

$$D_k^{0s} = \frac{tE_k^0 \kappa}{2(1+\nu)} \begin{bmatrix} 1 & 0 \\ 0 & 1 \end{bmatrix}$$

The sensitivities of objective function  $C$  with respect to densities for multi-material topology optimization of Reissner-Mindlin plates can be written by using the adjoint equation (Bendsøe and Kikuchi 1988) as follows

$$\frac{\partial C}{\partial \alpha_a^e} = -\mathbf{U}_e^T \frac{\partial \mathbf{K}^e}{\partial \alpha_a^e} \mathbf{U}_e \quad (15)$$

with

$$\frac{\partial \mathbf{K}^e}{\partial \alpha_a^e} = \frac{\partial}{\partial \alpha_a^e} \left[ \sum_{r=\{b,s\}} \int_{\Omega^e} \mathbf{B}_r^T \left( \sum_{k=1}^{n+1} \alpha_k^p \mathbf{D}_k^{r0} \right) \mathbf{B}_r d\Omega \right] \quad (16)$$

$$= p\alpha_a^{p-1} \sum_{r=\{b,s\}} \int_{\Omega^e} \left[ \mathbf{B}_r^T (\mathbf{D}_a^{r0} - \mathbf{D}_b^{r0}) \mathbf{B}_r \right] d\Omega$$

where  $\mathbf{B}_r$  with  $r=\{b,s\}$  are respectively strain-displacement matrix of bending and shear.  $\alpha_a^e$  and  $\mathbf{U}_e$  are the density of phase 'a' and the element displacement vector of element  $e$ -th, respectively.

In order to ensure existence of solutions to topology optimization problem and to avoid the formation of checkerboard patterns, a filtering technique on the resulting design is proposed (Andreassen *et al.* 2011). In this study, the filtered sensitivity of compliance with respect to density of phase 'a' of element  $e$ -th are derived as follows

$$\frac{\partial C}{\partial \alpha_a^e} = \frac{\sum_i H_{ei} \alpha_{ai}^e \frac{\partial C}{\partial \alpha_a^e}}{\alpha_a^e \sum_i H_{ei}} \quad (17)$$

where  $H_{ei} = r_{\min} - \text{dist}(e, \{f \in N \mid \text{dist}(e, f) \leq r_{\min}\})$  is a convolution operator.  $r_{\min}$  is the filter radius and  $\text{dist}(e, f)$  is the distance between the center of element  $e$  and center of element  $f$ .

## 4. Computational procedures of the present method

A briefly summarized computational procedures of the present multi-material topology optimization is shown in Fig. 4. This procedure describes optimality criteria-based alternating active-phase algorithm using Gauss-Seidel iteration version of multi-material. In addition, multi-material topology optimization for a thick plate structure by using Reissner-Mindlin plate theory is considered. To perform finite element analysis, the geometry, material properties, and loading and boundary conditions are determined. The stiffness matrix  $\mathbf{K}$  can be calculated through two components  $\mathbf{K}_b^e$  and  $\mathbf{K}_s^e$  by Eq. (7). By linear static analysis  $\mathbf{K}\mathbf{U}=\mathbf{F}$ , displacements can be obtained. By using Eq. (16), the sensitivity analysis of objective with respect to element design variables is calculated, and then the sensitivity filtering is applied. For the next step, design variables of a binary sub-problem are updated, and the iterative process continues until the desired optimum convergence conditions such as the reach of the minimum of compliance or the given number of iterations.

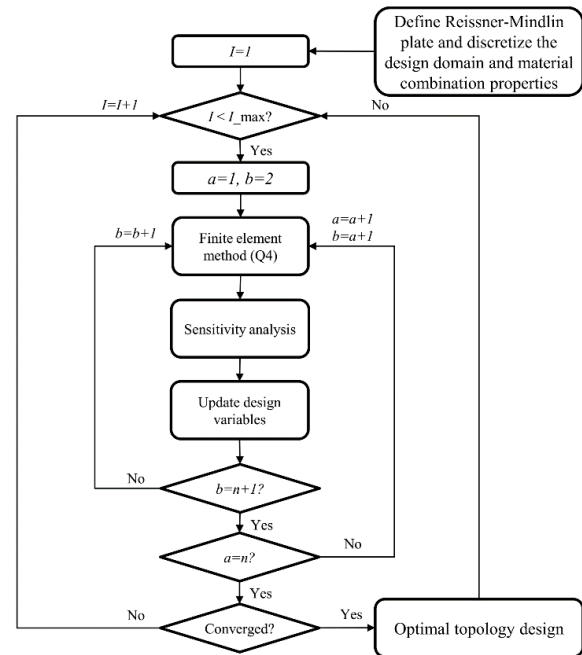


Fig. 4 Flowchart of multi-material topology optimization procedure for thick plates using alternating active-phase algorithm

Table 1 Multi-material properties

Material properties	Number of materials			
	(a) One	(b) Two	(c) Three	(d) Four
Young's modulus	$E_r^0 = 2e5$	$E_r^0 = 2e5, E_b^0 = 4e5$	$E_r^0 = 2e5, E_b^0 = 4e5$ $E_g^0 = 8e5$	$E_r^0 = 2e5, E_b^0 = 4e5$ $E_g^0 = 4e5, E_{bl}^0 = 1e6$
Volume fraction (30%)	$V_r = 30\%$	$V_r = 10\%, V_b = 20\%$	$V_r = 5\%, V_b = 10\%$ $V_g = 15\%$	$V_r = 3\%, V_b = 7\%$ $V_g = 9\%, V_{bl} = 11\%$
Volume fraction (50%)	$V_r = 50\%$	$V_r = 20\%, V_b = 30\%$		
Volume fraction (70%)	$V_r = 70\%$	$V_r = 30\%, V_b = 40\%$		

5. Numerical examples

In this section, Reissner-Mindlin thick plate structures subjected to a concentrated bending force are treated for multiphase topology optimization. The design domain is modeled as a square plate finite element (Q4) 40×40 mesh. The dimension of the structure is 30×30 and the plate's thickness is constant to be nominal value of 3. The magnitude of force  $F = 200$ . The problem situation is shown in Fig. 5. The penalization factor for interpolating elasticity properties of stiffness is equal to 3 for all materials. The optimized topology results are investigated for dependency degrees of boundary conditions, various materials and Poisson's ratio. The material is assumed to be isotropic. Young's modulus and volume fraction parameters for each material is presented in Table. 1, where the indicators  $r, b, g$  and  $bl$  denote red, blue, green and black colors, respectively. Note that Young's modulus and volume fraction of void are respectively selected  $V_v = 1 - \sum_{k \neq v} V_k$  for all examples.

5.1 Topology results of single material Reissner-Mindlin plates

5.1.1 Dependency of boundary condition

At first, optimized topology design results are investigated for different support conditions, i.e., fully clamped (C-C-C-C), fully simply supported (S-S-S-S) and mixed boundary conditions (C-S-C-S, C-F-C-F, here F: free) by using single material. Poisson's ratio of 0.3 is used. Figs. 6-9 clearly demonstrate boundary conditions and

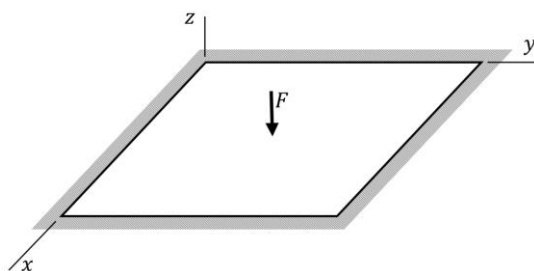


Fig. 5 Flowchart of multi-material topology optimization procedure for thick plates using alternating active-phase algorithm

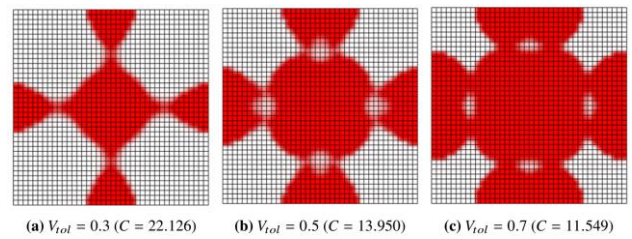


Fig. 6 Optimized topology results for thick plates (C-C-C-C) with single material and Poisson's ratio of 0.3

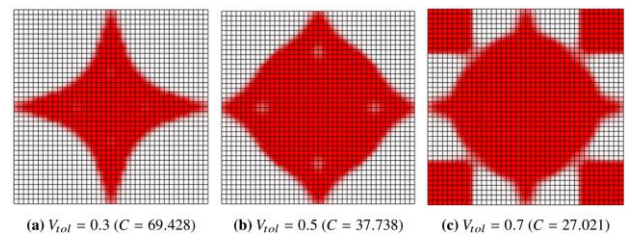


Fig. 7 Optimized topology results for thick plates (S-S-S-S) with single material and Poisson's ratio of 0.3

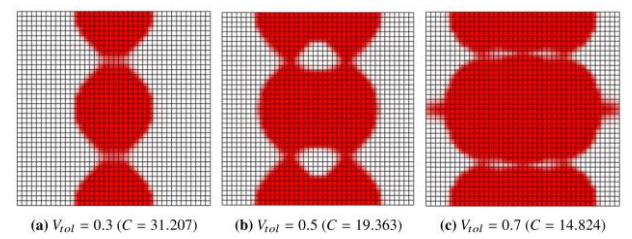


Fig. 8 Optimized topology results for thick plates (C-S-C-S) with single material and Poisson's ratio of 0.3

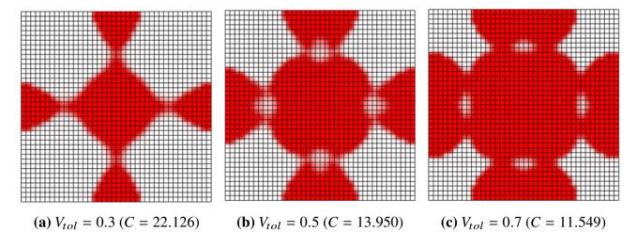


Fig. 9 Optimized topology results for thick plates (C-F-C-F) with single material and Poisson's ratio of 0.3

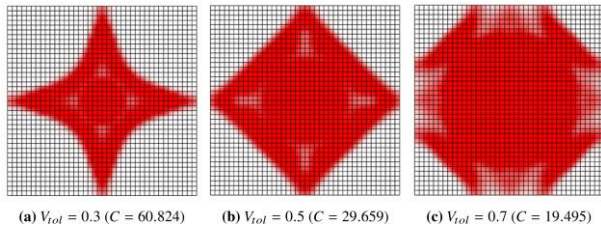


Fig. 10 Optimized topology results for thick plates (S-S-S) with single material and Poisson's ratio of 0.6

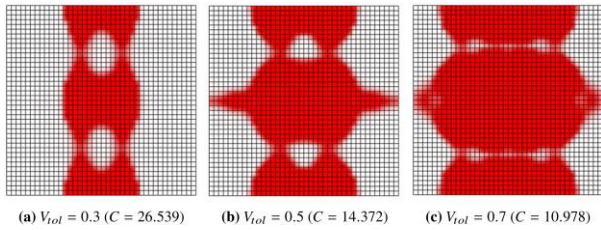


Fig. 11 Optimized topology results for thick plates (C-S-C-S) with single material and Poisson's ratio of 0.6

volume fraction result in different optimal topologies of single material Reissner-Mindlin plates. Fig. 12 presents convergence histories of objective function in case different boundary conditions.

5.1.2 Dependency of Poisson's ratio

The effect of Poisson's ratio is considered on optimal single material Mindlin plates. Two boundary condition cases S-S-S-S and C-S-C-S are applied. Figs. 10 and 11 depicts optimal topologies for two cases of Poisson's ratio values those ratios equal to 2, particularly, they are 0.3 and 0.6. Compared with optimal results of Poisson's ratios in Figs. 7 and 8, these results differ considerably. Fig. 13 shows the convergence histories of objective function in case different Poisson's ratio. As can be seen, optimal topologies of Reissner-Mindlin plates depend on material properties such as Poisson's ratio.

5.2 Topology results of two materials Reissner-Mindlin plates

5.2.1 Dependency of boundary condition

Similar to single material examples, four boundary condition cases are investigated. Poisson's ratio of 0.3 is used. The final optimal designs is shown in Figs. 14-17. In this example, stiff materials are used. Compared to single material case, the most different optimal topology is obtained in case fully simply supported boundaries (Figs. 15(b) and 15(c)). The distribution of materials in these cases is concentrated at corners. It means that the influence, when more materials are used, is dramatic. Fig. 20 presents the convergence histories of objective function for two materials in case different boundary conditions. As can be seen, similar to single material, the converged compliance in C-C-C-C always takes higher than those of the rest cases of boundary conditions.

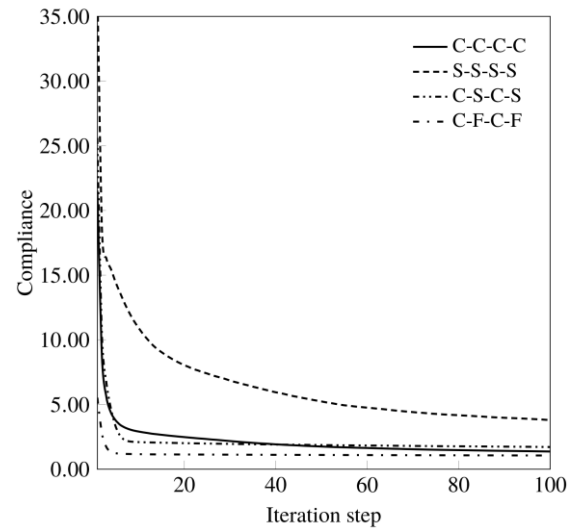


Fig. 12 Convergence histories of objective function in Section 5 with volume fraction of 0.3 and Poisson's ratio of 0.3

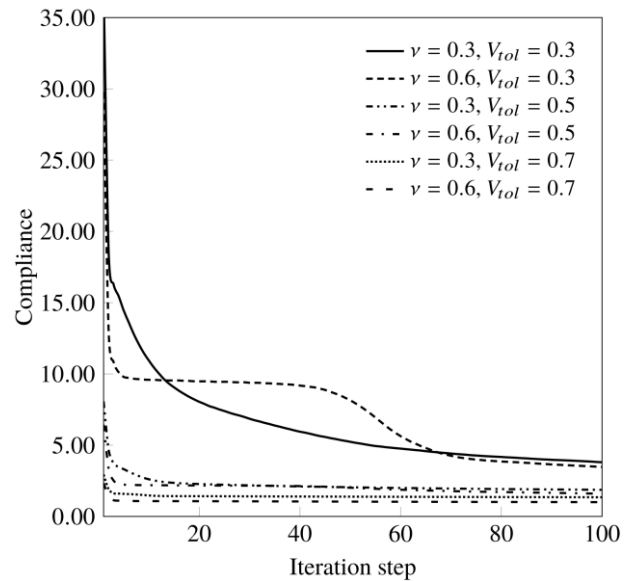


Fig. 13 Convergence histories of objective function in Section 5 for a fully simply supported boundary condition case

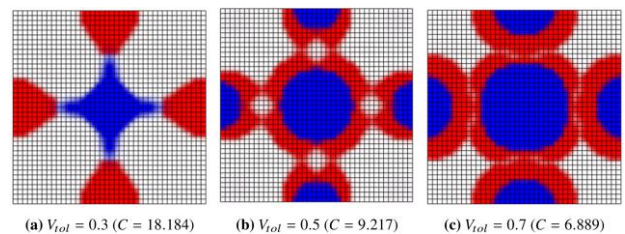


Fig. 14 Optimized topology results for thick plates (C-C-C-C) with two materials and Poisson's ratio of 0.3

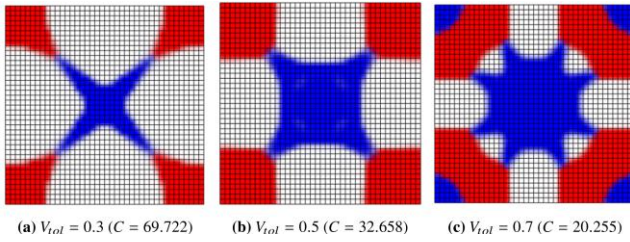


Fig. 15 Optimized topology results for thick plates (S-S-S-S) with two materials and Poisson's ratio of 0.3

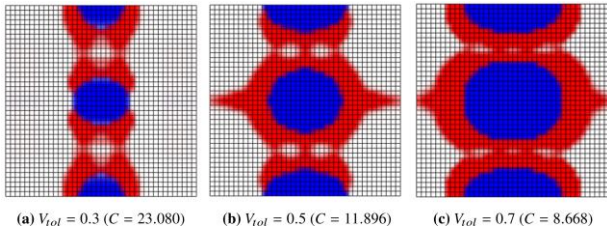


Fig. 16 Optimized topology results for thick plates (C-S-C-S) with two materials and Poisson's ratio of 0.3

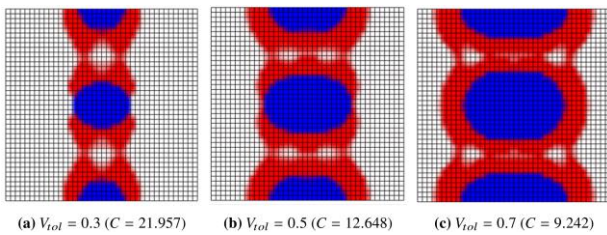


Fig. 17 Optimized topology results for thick plates (C-F-C-F) with two materials and Poisson's ratio of 0.3

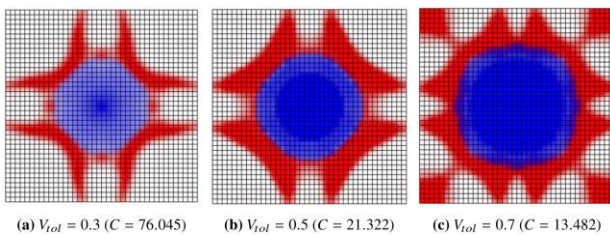


Fig. 18 Optimized topology results for thick plates (S-S-S-S) with two materials and Poisson's ratio of 0.6

5.2.2 Dependency of Poisson's ratio

The effect of Poisson's ratio on Mindlin plates with two boundary condition cases such as S-S-S-S and C-S-C-S by using two materials is shown in Figs. 18 and 19. They depict the optimum topology for Poisson's ratio of 0.6. In comparisons with optimal results of Poisson's ratio of 0.3 in Figs. 15 and 16, differences of topologies are much larger, in particular, in the fully simply supported case. Fig. 21 shows the convergence histories of objective function in case different Poisson's ratios.

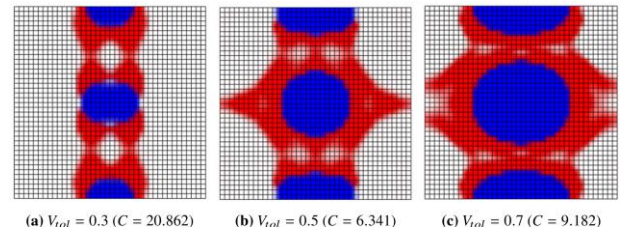


Fig. 19 Optimized topology results for thick plates (C-S-C-S) with two materials and Poisson's ratio of 0.6

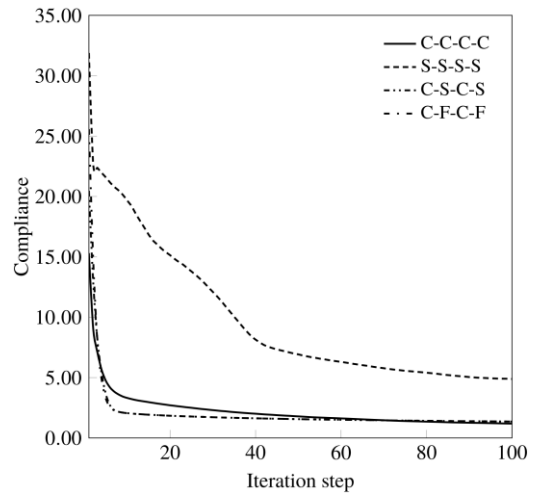


Fig. 20 Convergence histories of objective function in Section 5 with total volume fraction of 0.3 and Poisson's ratio of 0.3

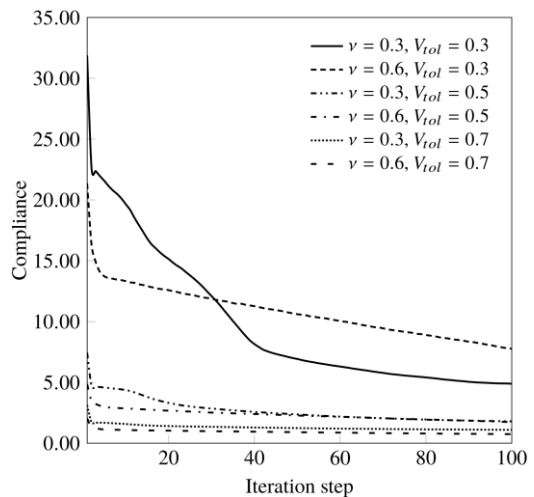


Fig. 21 Convergence histories of objective function in Section 5 for a S-S-S-S boundary condition case

5.3 Topology results of three to four materials Reissner-Mindlin plates

A fully clamped plate with four cases of material is considered for topology optimization. Optimal results are shown in Fig. 22 with volume fraction of 0.3 and Poisson's

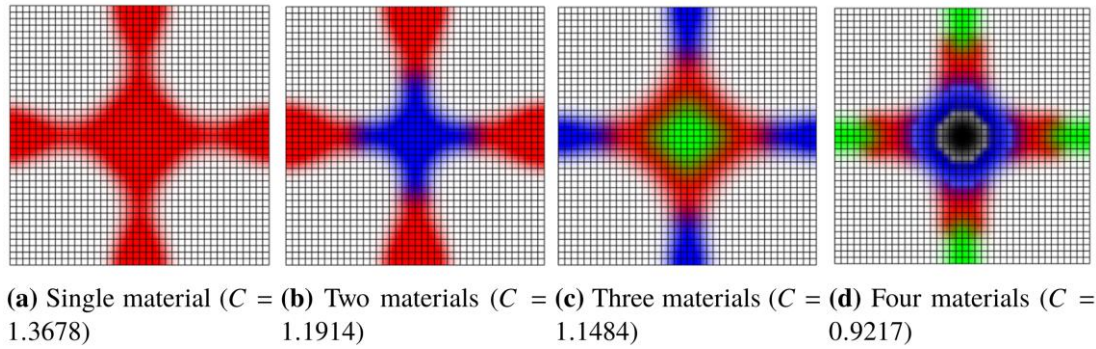


Fig. 22 Optimized topology results for thick plates (C-C-C-C) with from one to four materials with volume fraction of 0.3 and Poisson's ratio of 0.3

of bending

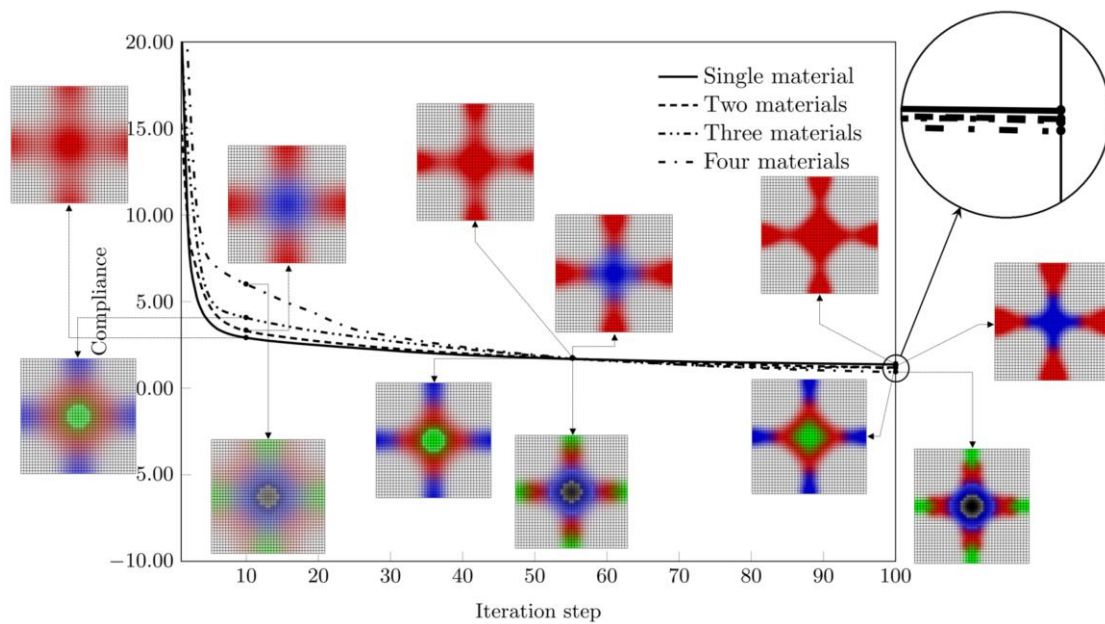


Fig. 23 Convergence histories of objective function in Section 5 with total volume fraction of 0.3 and Poisson's ratio of 0.3 (C-C-C-C)

ratio of 0.3. As can be seen, stiff materials are automatically assigned within strong stress concentration regions such as loading point and clamped boundary areas. In this example, applied loading areas have more influence on stiff material assignment than that of clamped boundary areas. Fig. 23 describes convergence histories of objective function (compliance) and intermediate topologies at several iterations of four material cases. Within the same amount of total material, multi-material can produce stiffer structure than single material.

and shear behaviors are developed to apply to the presence of topology optimization method. Numerical applications verify multi-material optimal topologies depending on boundary conditions, Poisson's ratio, and the number of materials according to Reissner-Mindlin plates. Moreover, this study shown that multi-material topology optimization method by using one or two additional stiff materials not only saves areas of initial structures but also gets higher stiffness than single material structures.

**6. Conclusions**

This study presents a novel numerical results by using topology optimization for smart plate-like-structures based on Reissner-Mindlin plate theory by using multiple materials. Adjoint sensitivity formulations for both multiphase material densities and Reissner-Mindlin plates

**Acknowledgments**

This research was supported by a grant (NRF-2017R1A4A1015660) from NRF (National Research Foundation of Korea) funded by MEST (Ministry of Education and Science Technology) of Korean government.

## References

- Alonso, C., Ansola, R. and Querin, O.M. (2014), "Topology synthesis of multi-material compliant mechanisms with a sequential element rejection and admission method", *Finite Elem. Anal. Des.*, **85**, 11-19.
- Andreassen, E., Clausen, A., Schevenels, M., Lazarov, B.S. and Sigmund, O. (2011), "Efficient topology optimization in matlab using 88 lines of code", *Struct. Multidiscip. O.*, **43**(1), 1-16.
- Banh, T.T. and Lee, D.K. (2018), "Multi-material topology optimization design for continuum structures with crack patterns", *Compos. Struct.*, **186**, 193-209.
- Belblidiaa, F., Lee, J.E.B., Rechakb, S. and Hinton, E. (2001), "Topology optimization of plate structures using a single- or three-layered artificial material model", *Adv. Eng. Softw.*, **32**, 159-168.
- Bendsøe, M. and Kikuchi, N. (1988), "Generating optimal topologies in structural design using a homogenization method", *Comput. Method. Appl. M.*, **71**(2), 197-224.
- Bendsøe, M.P. and Sigmund, O. (1999), "Material interpolation schemes in topology optimization", *Arch. Appl. Mech.*, **69**, 635-654.
- Blasques, J.P. and Stolpe, M. (2012), "Multi-material topology optimization of laminated composite beam cross sections", *Compos. Struct.*, **94**(11), 3278-3289.
- Chen, Y., Zhou, S. and Li, Q. (2009), "Computational design for multifunctional microstructural composites", *Int. J. Modern Phys. B*, **23**, 1345-1351.
- Chen, Y., Zhou, S. and Li, Q. (2010), "Multiobjective topology optimization for finite periodic structures", *Comput. Struct.*, **88**, 806-811.
- Goncalves, J.F., Fonseca, J.S. and Silveira, O.A. (2016), "A controllability-based formulation for the topology optimization of smart structures", *Smart Struct. Syst.*, **17**(5), 773-793.
- Goo, S.Y., Wang, S.Y., Hyun, J.Y. and Jung, J.S. (2016), "Topology optimization of thin plate structures with bending stress constraints", *Comput. Struct.*, **175**, 134-143.
- Kutyłowski, R. and Szwachłowicz, M. (2013), "Special kind of multimaterial topology optimization", *Arch. Civil. Mech. Eng.*, **13**, 334-344.
- Lee, D. and Shin, S. (2015a), "Optimising node density-based structural material topology using eigenvalue of thin steel and concrete plates", *Mater. Res. Innov.*, **19**, 1241-1245.
- Lee, D. and Shin, S. (2015b), "Optimising structural topology patterns using regularization of heaviside function", *Struct. Eng. Mech.*, **55**(6), 1157-1176.
- Lee, D., Kim, Y.W., Shin, S.M. and Lee, J.H. (2016), "Real-time response assessment in steel frame remodeling using position-adjustment drift-curve formulations", *Automat. Constr.*, **62**, 57-67.
- Liu, J. and Ma, Y. (2016), "A survey of manufacturing oriented topology optimization methods", *Adv. Eng. Softw.*, **100**, 161-175.
- Lund, E. (2009), "Buckling topology optimization of laminated multi-material composite shell structures", *Compos. Struct.*, **91**(2), 158-167.
- Noha, J.Y. and Yoon, G.H. (2012), "Topology optimization of piezoelectric energy harvesting devices considering static and harmonic dynamic loads", *Adv. Eng. Softw.*, **53**, 45-60.
- Olyaie, M.S. and Razfar, M. (2013), "Numerical characterizations of a piezoelectric micromotor using topology optimization design", *Smart Struct. Syst.*, **11**(3), 241-259.
- Sigmund, O. and Torquato (1997), "Design of materials with extreme thermal expansion using a three-phase topology optimization method", *J. Mech. Phys. Solids*, **45**, 1037-1067.
- Tavakoli, R. and Mohseni, S. (2014), "Alternating active-phase algorithm for multimaterial topology optimization problems: a 115-line matlab implementation", *Struct. Multidiscip. O.*, **49**, 621-642.
- Vatanabea, S.L., Lippia, T.N., de Limab, C.R., Paulinoc, G.H. and Silva, E.C. (2016), "Topology optimization with manufacturing constraints: A unified projection-based approach", *Adv. Eng. Softw.*, **100**, 97-112.
- Xia, Q. and Wang, M.Y. (2008), "Topology optimization of thermoelastic structures using level set method", *Comput. Mech.*, **42**, 837-857.
- Yan, K., Cheng, G. and Wang, B.P. (2016), "Topology optimization of plate structures subject to initial excitations for minimum dynamic performance index", *Struct. Multidiscip. O.*, **53**, 623-633.
- Yun, K.S. and Youn, S.K. (2017), "Multi-material topology optimization of viscoelastically damped structures under time-dependent loading", *Finite Elem. Anal. Des.*, **123**, 9-18.
- Zhou, S. and Wang, M. (2006), "3D multi-material structural topology optimization with the generalized cahn-hilliard equations", *Comput. Model. Eng. Sci.*, **16**, 83-101.
- Zhou, S. and Wang, M. (2007), "Multimaterial structural topology optimization with a generalized Cahn-Hilliard model of multiphase transition", *Struct. Multidiscip. O.*, **33**, 89-111.

CC